On the importance of the humidity flux for the surface mass balance in the accumulation zone of the Greenland Ice Sheet

Laura J. Dietrich[1], Hans Christian Steen-Larsen[1], Sonja Wahl[1,3], Anne-Katrine Faber[1], and Xavier Fettweis[2]

[1]Geophysical Institute, University of Bergen, and Bjerknes Center for Climate Research, Norway
[2]University of Liège, Belgium
[3]School of Architecture, Civil and Environmental Engineering, Ecole Polytechnique Fédérale de Lausanne, Switzerland

Correspondence:
Laura J. Dietrich (Laura.dietrich@uib.no)
Hans Christian Steen-Larsen (Hans.Christian.Steen-Larsen@uib.no)

Abstract. It is highly uncertain how the humidity flux between the snow surface and the atmosphere contributes to the surface mass balance (SMB) of the interior Greenland Ice Sheet (GrIS). Due to sparse observations, evaluations of the simulated humidity flux are limited. Model-based estimates of the humidity flux contribution to the SMB are, therefore, unconstrained and even disagree in magnitude and sign. In this study, we evaluate the regional climate model MAR at the EGRIP (East

5 Greenland Ice-Core Project) site in the accumulation zone of the GrIS. We use a combined dataset of continuous one-level bulk estimates of the humidity flux covering the period 05/2016–08/2019 and direct eddy-covariance humidity flux measurements from all four summer seasons. In summer, we document a bias of too little sublimation (-1.3 W m^{-2}) caused by a cold bias in both air and surface temperature leading to a reduced humidity gradient. In winter, MAR overestimates deposition by about one order of magnitude. This is a consequence of an overestimated temperature gradient in too stable atmospheric conditions

10 compared to observations. Both systematic errors cause a large discrepancy in the annual net humidity flux between the model and observations of -9 mm w. eq. yr^{-1}. Remarkably, the simulated net annual humidity flux contributes positively to the SMB, contrary to observations documenting a net sublimation flux. We correct the systematic errors by applying a simple but effective correction function to the simulated latent heat flux. Using this correction, we find that 5.1 % of the annual mass gain at the EGRIP site sublimates again, and 4.3 % of the total mass gain is deposited vapor from the near-surface air. The estimated

15 net humidity flux contribution to the annual SMB is about -1 % (net sublimation) compared to +5.6 % for the uncorrected simulation. In summer, the corrected MAR simulation shows that deposition accounts for 9.6 % of the total mass gain and that 31 % of the total mass gain at the EGRIP site sublimates again. The net fluxes contribute to -32 % of the summer SMB. These results demonstrate that the humidity flux is a major driver of the summer SMB in the accumulation zone of the GrIS and highlight that even small changes could increase its importance for the annual SMB in a warming climate.
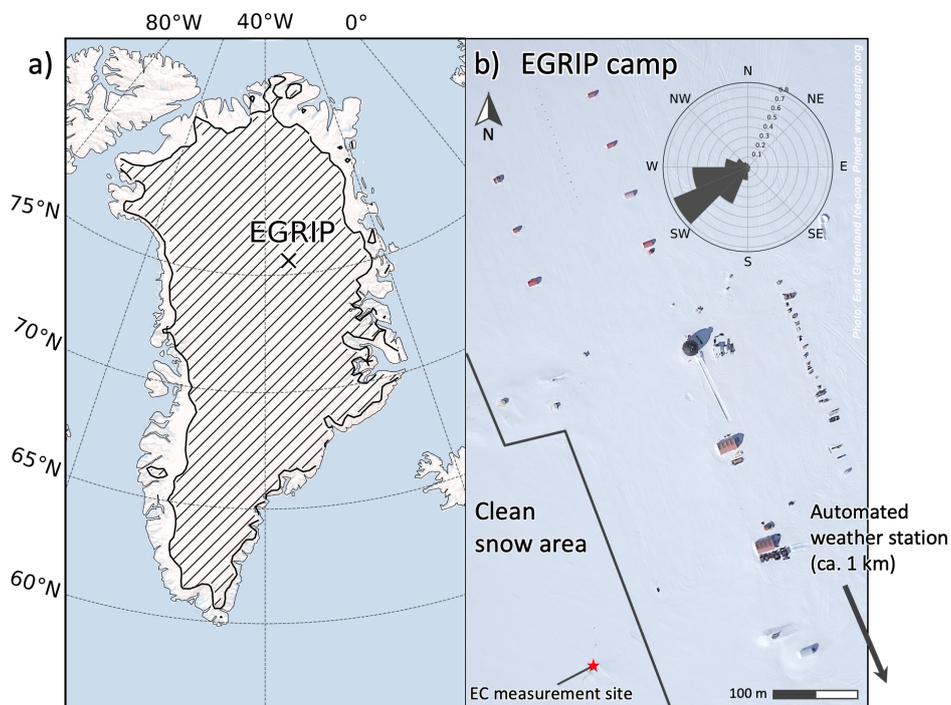
Figure 1. Model domain and accumulation zone (SMB$_{2016-2019}$ > 0, hatched area) for the MAR model simulation (a) and areal overview of the EGRIP (East Greenland Ice-Core Project) field site (b). The wind rose in (b) shows the normalized distribution of wind directions in the observational period (5/2016–8/2019).

1 Introduction

The Greenland Ice Sheet (GrIS) is the second-largest freshwater storage on Earth and loses mass at an increasing rate contributing to about 13.5 mm global mean sea level rise since 1992 (Fox-Kemper et al., 2021). The SMB and its drivers play an essential role in this mass loss (Mouginot et al., 2019). Quantifying all processes influencing the SMB is key to predicting the evolution of the GrIS in a warming climate. The humidity flux directly impacts the SMB by removing snow through evaporation/sublimation or adding mass by condensation/deposition. In the accumulation zone of the GrIS (Fig. 1 a), where temperatures typically stay below the freezing point throughout the year, sublimation is the only process that transports mass from the ice sheet to the atmosphere. In addition, long surface exposure times in the accumulation zone raise the potential of the humidity flux to impact the snow structure (Casado et al., 2021) and its isotopic composition (Wahl et al., 2022). Accurately simulating the SMB of the accumulation zone of the GrIS and the surface snow properties thus requires an accurate representation of the surface humidity flux in climate and snowpack models.

Regional climate model studies suggest that the annual contribution of the humidity flux to the SMB of the GrIS is minor. This is because the low temperatures above the GrIS lead to a relatively small humidity flux and because of the partial com-

pensation of sublimation and deposition (Cullen et al., 2014). However, in a warming climate, the counteracting contributions
35   of sublimation and deposition may shift (Boisvert et al. (2017), Zolles and Born (2021)) and as the increasing temperatures
amplify the humidity flux, they might gain importance in the future SMB.

Estimating the current contribution of the humidity flux to the SMB requires reliable observational datasets that span at least
a few years. However, observing the turbulent humidity flux in the accumulation zone of the GrIS is challenging due to its
40   remote location and cold and dry atmospheric conditions. Reliable datasets are therefore sparse with low temporal and spatial
coverage, and only a few datasets of humidity flux records span multi-annual periods. The humidity flux can be estimated from
measuring the humidity gradient and other meteorological parameters following a bulk approach, or directly measured using
the eddy-covariance method (EC, first described in Baldocchi (1988)). Generally, the humidity flux is reported as the latent
heat flux (LHF) which is the energy flux during a phase change of water. Box and Steffen (2001) used observed meteorological
45   variables from 20 GC-NET automated weather stations (AWS, Steffen et al. (1996)) in the accumulation zone of the GrIS
during 1995-1999 and estimated sublimation to be responsible for either 12 % or 23 % of precipitation loss following two dif-
ferent calculation methods. Cullen et al. (2014) used bulk estimates of the LHF from two years (2000-2002) of meteorological
observations in the accumulation zone of the GrIS and estimated the mass gain from the humidity flux to be less than 2 % of
the annual accumulation. The wide range of these estimates demonstrates that it is challenging to reduce uncertainties in the
50   humidity flux contribution to the SMB of the GrIS accumulation zone due to the sparse spatial coverage of observations.

Most of the available multi-annual records of the LHF are indirectly derived from meteorological observations by calculating
the LHF following a one- or two-level bulk estimation method. Bulk estimates are based on the Monin-Obukhov similarity
theory, which has limited accuracy under stable atmospheric conditions (Schlögl et al. (2017); Cullen et al. (2007)). Previ-
55   ous observations from the accumulation zone found the atmospheric conditions to be primarily stable in winter and weakly
unstable during summer (Cullen and Steffen, 2001). Therefore, using a bulk Monin-Obukhov similarity approach to estimate
the LHF introduces large uncertainty in the contribution of the humidity flux to the SMB for locations such as the GrIS or
Antarctic Ice Sheet. Indeed, Town and Walden (2009) found for measurements at the South Pole station that the bulk approach
underestimates the LHF by 40–60 % compared to observations obtained using the direct EC method. Sigmund et al. (2022)
60   observed a three times smaller flux using a bulk approach compared to the EC method during a storm period at the Syowa S17
station in East Antarctica. They find a flux underestimation using a bulk approach of 16–20 % with blowing snow turned off
in their simulations and even 70–87 % when blowing snow is enabled. Blowing snow is initally deposited snow that is blown
up by wind and that is in suspension in the air up to several tens of meters above the ground. In addition, the bulk method
requires knowledge of the aerodynamic roughness length, which is usually unknown, and assumptions about the wind profile
65   must be made. In the EC method, the surface roughness length can be obtained directly from the turbulence measurements and
no assumptions regarding the wind profile are required to obtain the LHF. Therefore, the direct EC method is best for observing
the humidity flux in the accumulation zone of the GrIS with smaller errors under the prevailing slightly stable conditions in

polar regions.

70   To compensate for the sparse observations and to obtain spatial coverage in the accumulation zone, climate model simulations of the SMB are indispensable. Thus, most of the current estimates of the humidity flux contribution rely solely on model simulations. However, these model simulations are unconstrained as the parameterizations of humidity exchange processes at the snow surface for the accumulation zone have not been evaluated on neither intra- nor inter-annual time scales. Thus, the role that the humidity flux plays for the SMB of the interior GrIS remains unconstrained, if not completely unknown.

75

    This study addresses the uncertainty in regional climate model estimates of the humidity flux contribution to the SMB in the accumulation zone of the GrIS. We use a novel EC dataset of the humidity flux from the EGRIP drilling site during four summers (June and July 2016–2019) to evaluate the state-of-the-art regional climate model MAR (described in Section 2) for polar regions. Based on the evaluation, we apply a simple correction function, which allows us to constrain the model

80 simulations and to provide an improved estimate of the seasonal and annual humidity flux contribution to the SMB at the EGRIP site. Note that in this study, an upwards directed humidity flux (sublimation) is defined positive, causing a negative contribution (mass loss) to the SMB.

2   Data and Methods

Regional climate model MAR

85 To investigate the hydrological cycle over the GrIS, we use version v3.11 of the hydrostatic regional climate model MAR (Modèle Atmosphérique Régional, e.g., Fettweis et al. (2017)) and simulate the surface processes, and mass and energy balance in the period 2016–2019. MAR is a well-established model for SMB simulations over the GrIS (e.g. Fettweis et al. (2020), Goelzer et al. (2020)). We run MAR on a vertical resolution of 30 atmospheric layers between 1 m and the top of the atmosphere (0.1 hPa) with an increased resolution towards lower altitudes. We use a horizontal resolution of 30 km on a 66 x 113 grid

90 points domain (Fig. 1 a), which is a sufficient resolution to investigate the flat and orographically smooth top of the GrIS. For the comparison with the observational data from the EGRIP site the nearest grid cell is chosen. The simulations are calculated for a time step of 180 seconds, and MAR's output is given in hourly averages. The simulation is initialized and forced at its boundaries with 6-hourly data of the ERA-5 reanalysis product (Hersbach et al., 2020). The atmospheric model is coupled to the 1-D Surface Vegetation Atmosphere Transfer scheme SISVAT (Soil Ice Snow Vegetation Atmosphere Transfer, Fettweis

95 et al. (2005)), which simulates the snow-atmosphere interactions of energy and mass. The snowpack and snow properties are simulated based on an early version of the CROCUS snow model implemented in SISVAT. The blowing-snow module (Gallée et al. (2001), Amory et al. (2021)) was turned off in this study to exclude local redistribution of deposited snow from the SMB simulation at the EGRIP site. This allows extrapolating findings for the EGRIP site to more comprehensive parts of the accumulation zone of the GrIS.

Latent heat flux parameterization in MAR

The LHF in MAR is calculated using a one-level bulk parameterization. At the snow surface, saturation with respect to the snow surface temperature and a wind speed of zero is assumed. The LHF is calculated by

$$LHF = -\rho L_s \kappa^2 \frac{u}{\ln\left(\frac{z_u}{z_{u,0}}\right) - \Psi_u} \cdot \frac{q - q_s}{\ln\left(\frac{z_q}{z_{q,0}}\right) - \Psi_q} \tag{1}$$

where ρ is the air density, $L_s = 2.831 \cdot 10^6 \, \text{J kg}^{-1}$ the latent heat of sublimation and $\kappa \approx 0.4$ the von Kármán constant. u is the wind speed, and q the air specific humidity at the heights $z_u = 2\,\text{m}$ and $z_q = 2\,\text{m}$, respectively. In the MAR simulations, a constant roughness length for momentum of $z_{0,u} = 1.3 \cdot 10^{-4}\,\text{m}$ is used, which corresponds to the observed median in EC measurements during summer. The roughness length of moisture $z_{0,q}$ is derived following the parameterization by Andreas (1987) for snow surfaces. The stability correction functions for momentum Ψ_u and for moisture Ψ_q are calculated following Holtslag and De Bruin (1988) for stable atmospheric conditions and assuming $\Psi_q = \Psi_u$. For unstable conditions, the Businger-Dyer representation is used, described in Paulson (1970):

$$\Psi_u = 2 \cdot \ln\left(\frac{1+x}{2}\right) + \ln\left(\frac{1+x^2}{2}\right) - 2 \cdot \tan^{-1}(x) + \frac{\pi}{2}$$

and

$$\Psi_q = 2 \cdot \ln\left(\frac{1+x^2}{2}\right)$$

where $x = (1 - \gamma/\zeta)^{\frac{1}{4}}$ with the dimensionless stability parameter $\zeta = z_u/L$, where L is the Monin-Obukhov length and $\gamma = 16$ an empirically derived constant.

Meteorological data

Meteorological observations are obtained from an AWS as part of the Programme for Monitoring of the Greenland Ice Sheet (PROMICE, Fausto et al. (2021)). The AWS was installed in May 2016 and is regularly maintained. It provides continuous observations of wind speed, humidity, surface temperature, 2 m temperature, and solar and thermal radiation fluxes. In 2016–2019 the sensors had an average height of 2.3 m [2.6 m to 1.8 m] above the snow surface, and the meteorological data is compared to the model output at 2 m without correcting for the height difference, assuming it is insignificant.

Atmospheric eddy-covariance system

We evaluate the surface humidity flux in MAR using a dataset of direct EC measurements from the EGRIP site (Steen-Larsen et al., 2022). The EC data consists of 30-minute LHF averages for all summers (June and July) in 2016–2019. We use hourly averages which gives a total amount of 5304 data points. The EC system consists of a CSAT3 wind sensor combined with a KH20 hygrometer (both by Campbell Scientific) which are installed at a height of 1.80 m facing the prevailing wind direction (240°, Fig. 1 b). The EC system measures the three-dimensional wind speed (u,v,w), and the water vapor density q (kg m^{-3})

at a high sampling frequency of 20 Hz. In that way, the EC method directly measures the turbulent transport of moisture and the LHF can be derived by $LHF = \text{cov}(w, q) \cdot L_s$. We are confident in the EC measurements of the LHF used in this study
130 because three different EC systems were installed in 2019 to test the reliability of the EC method in polar conditions at EGRIP and the comparison showed excellent agreement (not shown in this study).

2.1 Site description

All measurements for the model evaluation were carried out as part of the deep ice core drilling project EGRIP (East Greenland Ice-Core Project). The EGRIP drilling site is located at 75° 38' N and 36° 00' W in the interior of the GrIS accumulation zone
135 at an approximate height of 2700 m above sea level. The local time (LT) is two hours behind the Coordinated Universal Time (UTC). Meteorological observations are provided by an AWS located about 1 km southeast of the EGRIP camp (Fig. 1 b). The EC system is set up in a dedicated clean snow area upstream of the prevailing wind direction from the EGRIP camp.

During the summer months of 2016–2019, the prevailing wind direction was west to north-west with an average wind
140 speed of 4.6 m s^{-1} (daily average between 1.1 and 8.9 m s-1), and the average 2 m air temperature was -9.4 °C (daily average between -22.6 and -1.9 °C) with the average diurnal cycle in summer (June and July) spanning -14.7 – -8 °C. All four years have similar meteorological conditions (Fig. A1), but 2016 and 2019 were slightly warmer and moister during summer, leading to generally higher LHF.

3 Results

145 ### 3.1 Evaluation of the regional climate model MAR

We evaluate the simulated LHF at EGRIP against the EC observations for all summers (June and July) in 2016–2019 in Fig. 2. MAR systematically underestimates the LHF with a mean bias of -1.3 W m^{-2}. In all four summers, the bias is consistently negative and independent of the time of day. Besides the bias, MAR captures the diurnal cycle well (Fig. 2 c). The simulated LHF has a similar diurnal range, spanning from -3.7 to 7.5 W m^{-2}, and the diurnal maximum and minimum are aligned with the
150 observations. During summer, the simulated daily mean LHF has a standard deviation of 1.79 W m^{-2}, similar to the observations ($STD_{\text{Obs, daily mean}} = 1.92$ W m^{-2}). The daily mean values of the simulated and observed LHF are only weakly correlated ($R = 0.27$). This goes along with a high non-systematic error in the daily mean LHF simulations with a root-mean-square error (RSME) of 2.66 W m^{-2}, equivalent to 1.39 times the observed standard deviation. MAR is only forced with the reanalysis at the domain's boundaries every six hours, and therefore, the exact timing of weather events may be shifted. On sub-diurnal
155 time scales, MAR performs slightly better during the night hours (6 pm - 6 am LT) with a correlation of $R = 0.25$ compared to $R = 0.20$ during the day hours (6 am - 6 pm LT, Fig. A2). Despite the high non-systematic error, MAR captures the distribution of the LHF remarkably well in the four summers of the observational period (Fig. 2 a,b). Similar to the observations, the distribution of the simulated LHF has a slightly right-skewed shape, spanning a range of -10 to 20 W m^{-2}, with 50 % of the
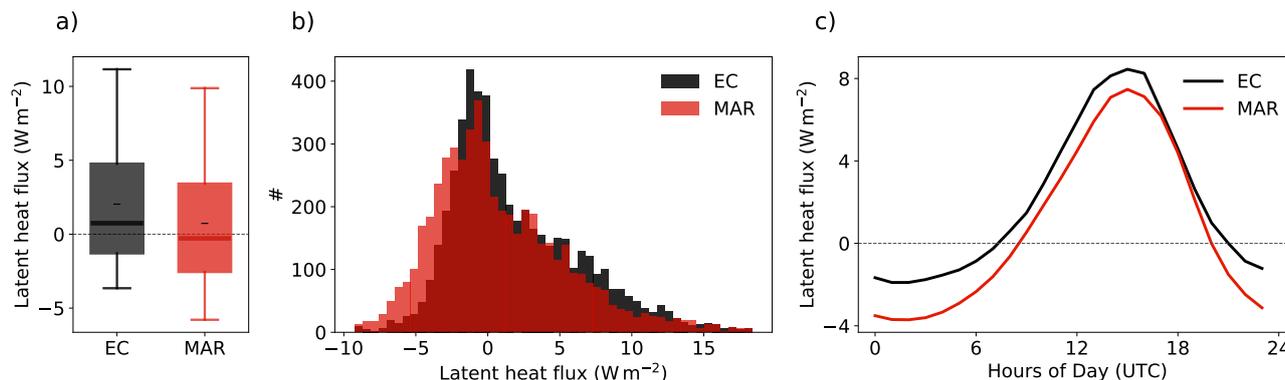
Figure 2. Distribution (a,b) and diurnal cycle (c) of the observed (EC, black) and simulated (MAR, red) hourly latent heat flux during all summers in the observational period (June and July 2016–2019) at the EGRIP location. In (a), black dashes (-) denote the mean, thick lines denote the median, boxes denote the 25th–75th percentile, and whiskers denote the 5th–95th percentile. Hours of the day in (c) are given in UTC, and the LT corresponds to UTC-2 h.

LHF being between -2.5 and $3.4\,\mathrm{W\,m^{-2}}$.

Fig. 3 shows the variables that have a direct impact on the LHF (Eq. 1) for the summer of 2019. The summer of 2019 is a good representative of the average summer in 2016–2019 (Fig. A3). MAR captures the daily wind speed ($R = 0.76$) and air density ($R = 0.79$) in both distribution and mean but fails to reproduce the daily specific humidity gradient Δq ($R = 0.28$), which is defined as the difference between q at 2 m height and the saturation specific humidity at the surface $q_{s,\mathrm{sat}}$. While in the observations, Δq is mostly negative, MAR simulates a net zero Δq leading to a bias in the humidity flux. Similar to the LHF, although the daily values of Δq differ from the observations, its diurnal cycle and the shape of the distribution are captured.

Estimating the humidity flux contribution to the the SMB requires LHF simulations in all seasons. However, there are no year-round direct EC flux measurements of the LHF available for the EGRIP site. To evaluate the LHF simulation in MAR beyond the summer months, we estimate the LHF from meteorological observations using a similar one-level bulk parameterization method as implemented in MAR. For the calculations we use a constant roughness length of $1 \cdot 10^{-5}\,\mathrm{m}$. This is a substantially smaller value than the median of the observed roughness length ($1.3 \cdot 10^{-4}\,\mathrm{m}$) but it provides best agreement with the direct EC observations of the LHF in summer. The LHF of the EC observations and the bulk estimate has a correlation of $R = 0.72$ after removing the diurnal cycle and an RMSE of $2.3\,\mathrm{W\,m^{-2}}$ (Fig. A4). This gives confidence in the bulk estimates despite the weakly stable conditions. Like in summer, the simulated LHF is biased towards deposition throughout the entire season (Fig. 4 a, Fig. 5 c). Nevertheless, MAR simulates a shape of the seasonal cycle similar to the observations with a monthly mean value correlation of 0.88 (Fig. 4 a). After removing the seasonal cycle, the correlation of the monthly mean values reduces to 0.31, with MAR performing better in spring ($R_{MAM} = 0.59$) and autumn ($R_{SON} = 0.80$) than in summer
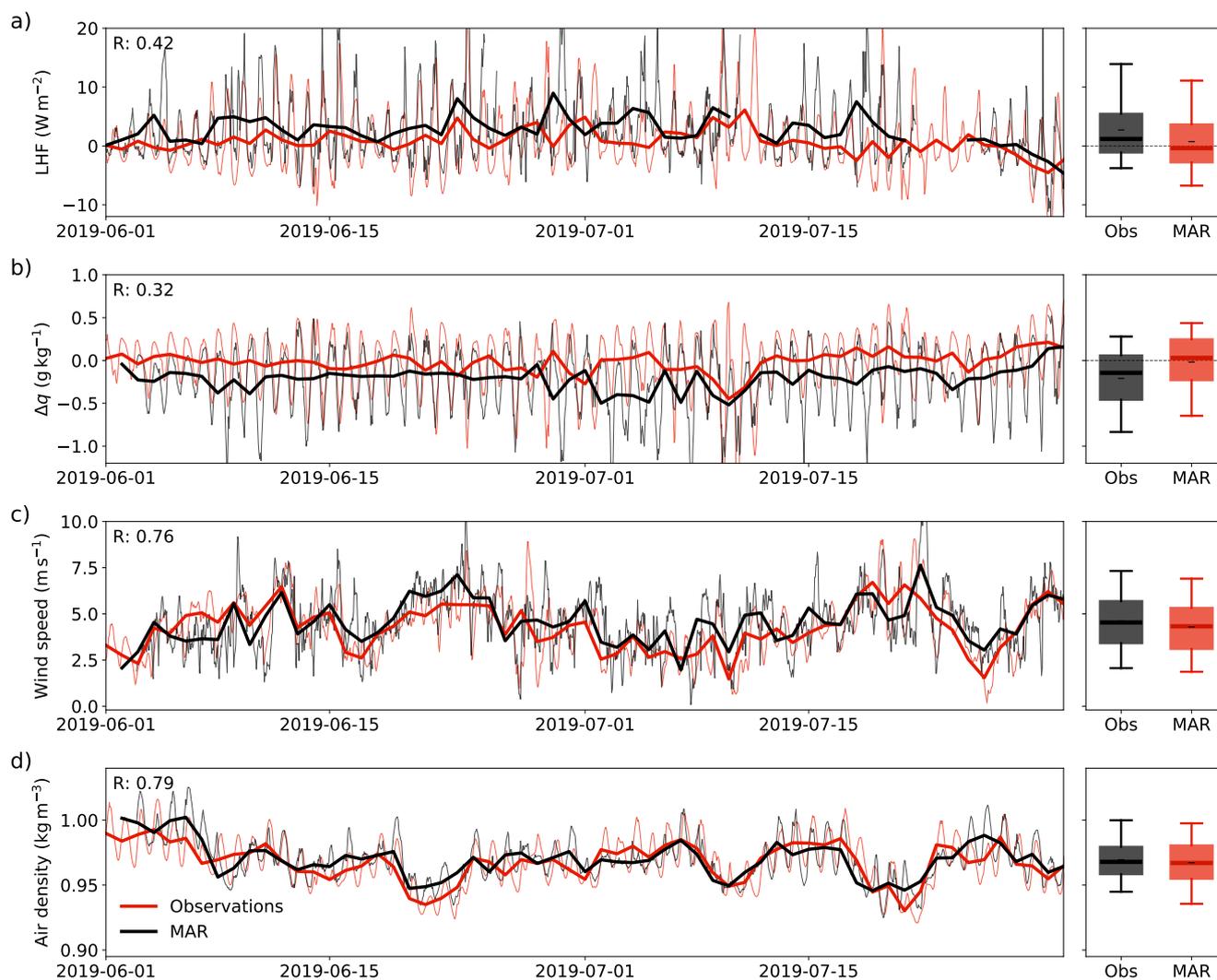
Figure 3. Time series of the latent heat flux (LHF, a), specific humidity gradient (Δq, b), wind speed (c), and air density (d) in the period 06/2019–07/2019 from observations (Obs, black) and MAR (red). The bold lines show daily averages, hourly data is plotted in thin lines. The boxplots (right) show the distribution of the hourly data presented in the time series plots (left). In the boxplots, black dashes (-) denote the mean, thick lines denote the median, boxes denote the 25th–75th percentile, and whiskers denote the 5th–95th percentile.
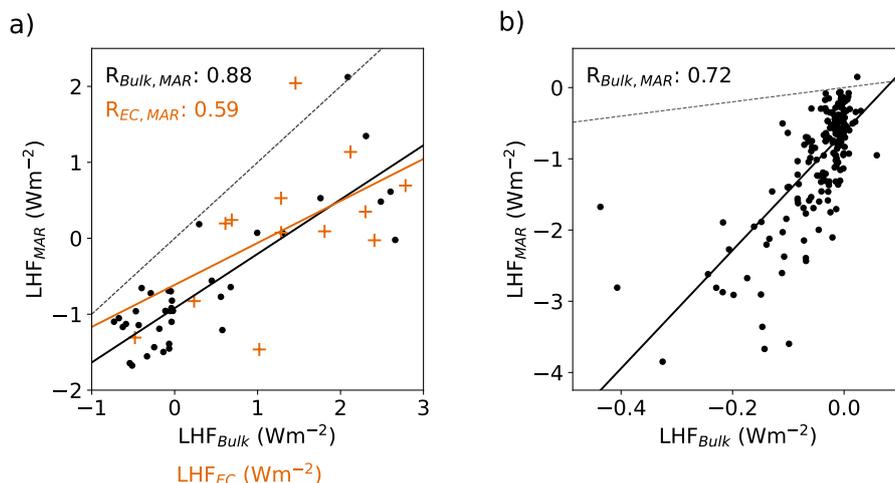
Figure 4. a) Comparison of the LHF monthly mean values for the bulk calculation (black dots) and EC measurements (orange crosses) to the MAR simulation. Note that there are only EC data available for May, June, July, and August. b) Comparison of the LHF daily mean values for the bulk calculation for all winters (December, January) in 2016-2019. Note that in winter the daily net fluxes are exclusively depositional. The grey dashed lines show the one-to-one lines.

($R_{JJA} = -0.19$) and winter ($R_{DJF} = 0.33$). Note that these seasonal correlations are only based on twelve values out of four

180 years per season. Daily mean values (after removing the seasonal cycle) have a correlation with the bulk estimate of $R = 0.42$ for the entire observational period.

A closer look at the systematic error in the seasonal cycle reveals a more complex cause than a simple offset. The distribution of the simulated LHF differs from the bulk estimate (Fig. 5). The simulations have a more right-skewed shape than the bulk

185 estimates, as the occurrence of negative fluxes is overestimated, and the occurrence of positive and small fluxes, close to zero, is underestimated. Contrary to summer, in winter, the magnitude of the simulated LHF is about one order of magnitude larger than the bulk estimate on both hourly (Fig. 6) and daily time scales (Fig. 4 b). The systematic error in winter is a factor rather than an offset.

190 We analyze the hourly and daily variability in MAR and observations in Fig. 6 for winter 2019, which is a good representative of an average winter in 2016–2019 (Fig. A5). The bulk estimate of the LHF has a low daily variability with mostly negative values close to zero for most of the winter except for isolated events. On the contrary, MAR simulates a relatively strong depositional flux. Despite the strong overestimation, MAR is consistent in the timing of the observed events, such that the daily mean correlation of the LHF is high ($R = 0.77$). Like in summer, the specific humidity gradient can explain the major part of

195 the LHF difference in winter between the observations and MAR (Fig. 6 b). Additionally, ρ shows a small bias (Fig. 6 d). The bias in ρ is caused by equal contributions of both a bias in pressure and temperature.
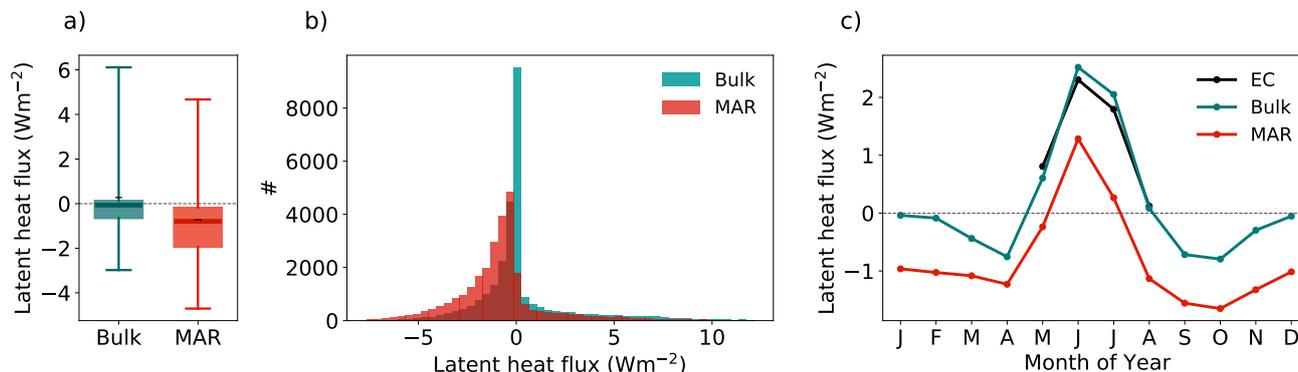
Figure 5. Distribution (a,b) and seasonal cycle (c) of the hourly latent heat flux calculated from observations (bulk, turquoise) and simulated (MAR, red) during the entire observational period (05/2016–08/2019). In (a), black dashes (-) denote the mean, thick lines denote the median, boxes denote the 25th–75th percentile, and whiskers denote the 5th–95th percentile.

3.2 Improved estimate of the SMB contribution

The evaluation in Section 3.1 shows that, in summer, MAR has a negative bias in the LHF while simulating a similar variability as observed. In winter, the bias diminishes, but MAR overestimates the magnitude of the LHF and, thus, overestimates both

200 the variability and the total deposition. These seemingly small systematic errors in the humidity flux lead to a mean difference of -9 mm w. eq. yr^{-1} in its contribution to the SMB at the EGRIP site (Fig. 7). In fact, MAR simulates a positive contribution (net deposition) to the annual SMB, while the observations show a slightly negative contribution (net sublimation). To obtain an improved estimate of the humidity flux contribution to the annual SMB, we propose a simple linear correction function $f(LHF_{\mathrm{MAR,\,corr}}) = m \cdot LHF_{\mathrm{MAR}} + b$ to correct for systematic errors in the simulated LHF.

205

The parameters m and b (Fig. 8) account for the two different types of systematic errors in MAR described above. The systematic error in the LHF simulation is mainly caused by systematic errors in the surface and 2 m temperature and their difference that affects the near-surface humidity gradient (see Sec. 3.2.1). Therefore, the correction function of the LHF simulation is based on $q_{s,\mathrm{sat}}$, which has a nonlinear dependence on the surface temperature (Clausius-Clapeyron). The factor m

210 depends on the inverse of $q_{s,\mathrm{sat}}$ and is normalized so that it varies between 1 in summer (June and July) and 0.1 in winter (December and January). Thus, there is no effect on the flux magnitude in summer but a flux magnitude reduction in winter by one order of magnitude. The bias correction b depends directly on $q_{s,\mathrm{sat}}$, and b varies between the observed bias value of 1.3 in summer and 0.1 (zero bias on January 1st) in winter.

215 As a result of the factor correction, the deposition during winter is strongly reduced, leading to a smaller mass gain (Fig. A8 c). During summer, the bias correction function shifts the LHF towards enhanced sublimation, and thus, the mass
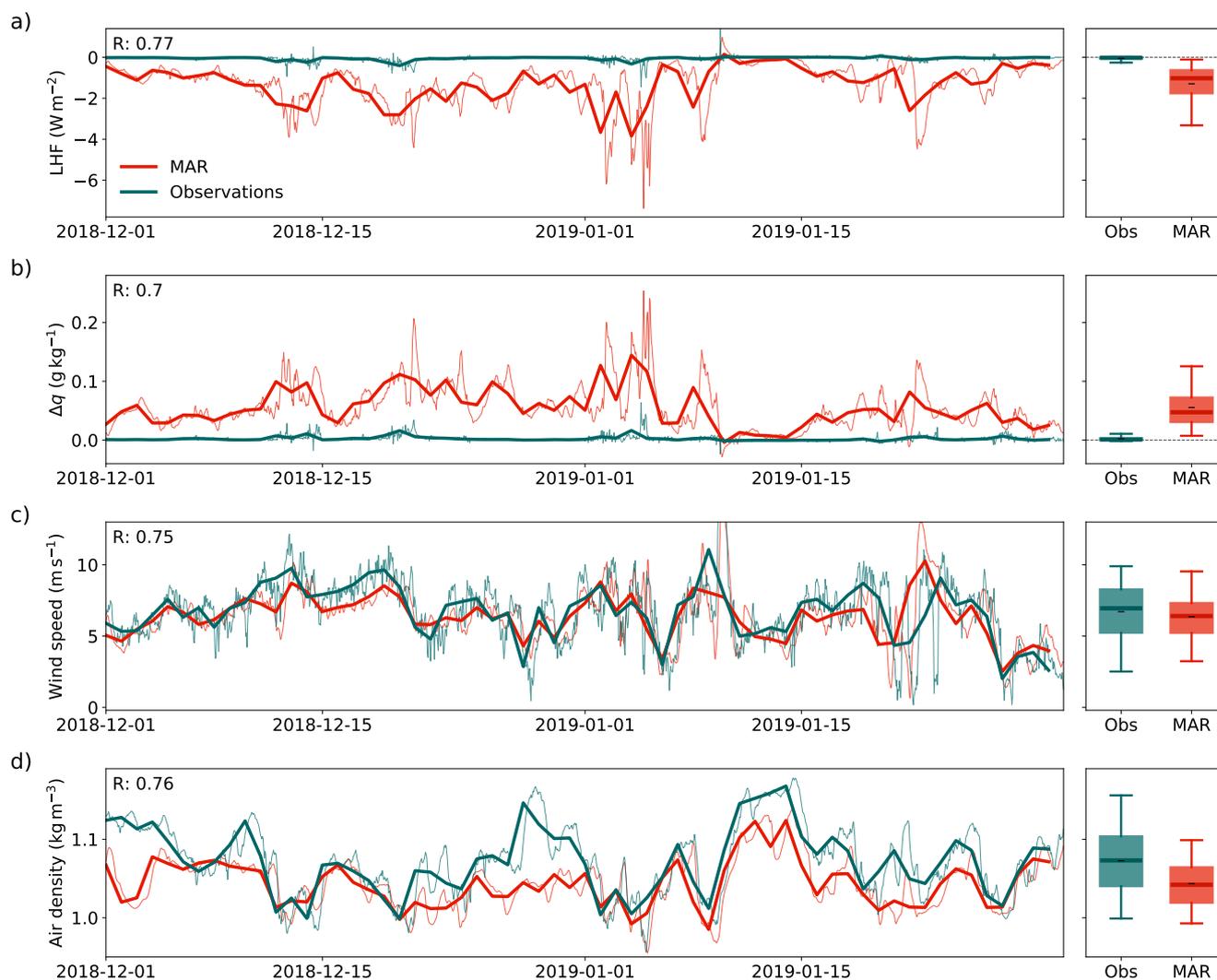
Figure 6. Time series (left) and distribution (right) of the latent heat flux (LHF, a), specific humidity gradient (Δq, b), wind speed (c), and air density (d) in the period 12/2018–01/2019 from observations (Obs, turquoise) and MAR (red). The bold lines show the daily averages of the hourly data (thin lines). The boxplots (right) show the distribution of the hourly data presented in the time series plots (left). In the boxplots, black dashes (-) denote the mean, thick lines denote the median, boxes denote the 25th–75th percentile, and whiskers denote the 5th–95th percentile.
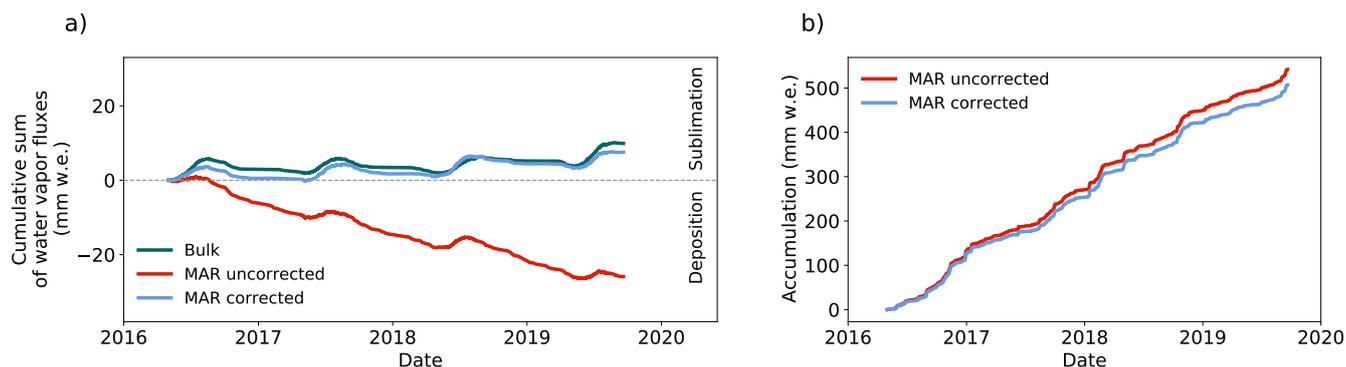
Figure 7. Left: Cumulative sum of the humidity flux from observations (dark green), simulated by MAR (red) and the corrected MAR simulation (blue) for the time period. Positive values correspond to a surface mass loss due to sublimation. Right: Cumulative sum of the simulated total accumulation (snowfall + deposition - sublimation) in MAR.
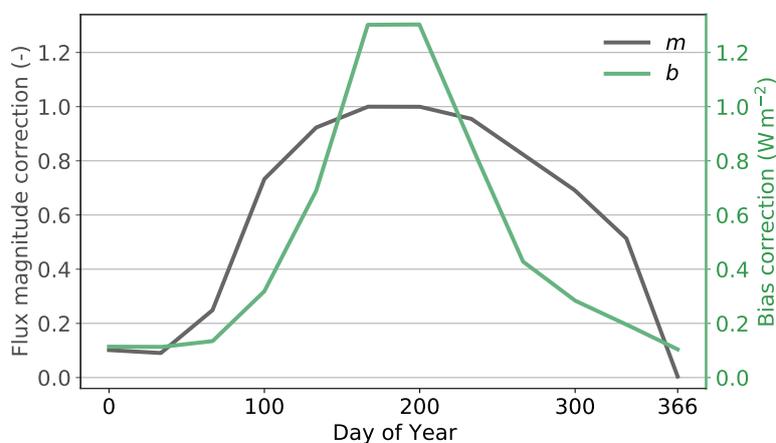
Figure 8. Annual cycle of the parameters m and b of the linear correction function for the simulated LHF.

loss is increased. We use the corrected LHF simulations in MAR and calculate the humidity flux contribution to the SMB at the EGRIP drilling site in the period 2016–2019 as well as the range for the individual years to estimate the inter-annual variability. By applying the correction, we find that contrary to MAR's uncorrected LHF simulation and previous estimates (e.g., Fettweis

220 (2007)), the net humidity flux at EGRIP is not negative but positive (Fig. 7 a), i.e., causes a net mass loss equivalent to -1 % of the annual SMB, while the uncorrected simulation shows a mass gain equivalent to +5.6 % of the annual SMB. In the corrected simulation 5.1 % [4 % to 6 %] of the annual mass gain (snowfall + deposition) sublimates again, and 4.3 % [3.2 % to 5.3 %] of the mass gain is deposited water vapor from the air. During summer, the amount of sublimated mass corresponds to 31 % [26 % to 34 %] of the total mass gain. Deposition accounts for 9.6 % [7.4 % to 12 %] of the mass gain during summer in MAR

225 (Fig. A6). The simulated net humidity flux contributes to 32 % [23 % to 37 %] of the summer SMB. Our results demonstrate that the humidity flux, in particular sublimation, has a major contribution to the summer SMB (Fig. A6), and that an accurate humidity flux representation in models is important for the simulation of the SMB over multi-annual time scales (Fig. 7 b).

3.2.1 Discussion

Regional climate models are key to estimating the SMB of the GrIS, as observations are challenging in polar environments.

230 Our evaluation shows that MAR captures all relevant processes driving the humidity flux and captures the distribution of the LHF remarkably well (Fig. A8). For many purposes in climate modeling, capturing the distribution of the humidity flux is more important than having a low random error. We conclude that MAR is a well-performing tool for humidity flux simulations in the accumulation zone of the GrIS when using an appropriate surface roughness length. However, even small systematic errors in the humidity flux can have large impacts on the SMB contribution on seasonal and annual time scales, with potential impacts

235 on the snow surface properties.

The seemingly small summer bias of -1.3 W m^{-2} in the uncorrected simulation leads to a three times smaller mass loss due to the humidity flux over the four summers compared to the corrected humidity balance (not shown). An error in the LHF could potentially be caused by an erroneous representation of three meteorological variables (Eq. 1): (1) the wind speed, (2) the air

240 density, and (3) the specific humidity gradient. In summer, the bias towards a smaller LHF is primarily driven by a bias in Δq towards smaller gradients and, to a lesser degree, by a small negative bias in both air density and wind speed. The bias in the Δq is caused by a cold bias in the surface temperature of -1.5 K, affecting the surface saturation specific humidity. The 2 m air temperature has a similarly strong bias (-1.2 K), however, MAR overestimates the relative humidity so that the distribution of the specific humidity at 2 m agrees with the observations. The cold biases in both the surface and the 2 m air temperature are

245 a direct consequence of a negative bias in the downward long-wave radiation flux linked to the cloud scheme implemented in MAR. Besides the systematic error, Δq explains 64 % of the non-systematic error in the daily LHF averages in summer as well.

In winter, the systematic error in the LHF is not a bias but a consistent overestimation of the LHF magnitude. Again, the wind speed is captured well by the model ($R = 0.72$, $RMSE = 0.73$ W m^{-2}) with only a small bias of 0.18 m s^{-1}. The bias in

250 the air density of -0.027 kg m^{-3} is a direct consequence of, first, a bias in the air pressure of -6.6 hPa and, second, an overesti-

mation of the 2 m air temperature by 3.67 K. However, the simulated air density is only about 2.7 % lower than the observations and is, hence, considered to have a small impact. Like in summer, it is thus mainly Δq that causes the systematic error in the LHF in winter. Moreover, Δq explains more than 90 % of the non-systematic error of the daily mean values in winter.

255   The specific humidity gradient is primarily driven by the temperature gradient due to the Clausius-Clapeyron relationship and, to a lesser degree, by the relative humidity. MAR also systematically underestimates the relative humidity during winter (not shown). However, this would counteract the LHF overestimation and is found to be insignificant compared to the impact of the temperature gradient. The simulated temperature gradient is on average overestimated by 2.93 K in winter, causing a strong overestimation of Δq. This is a consequence of a large bias in the simulated 2 m temperature (3.67 K), while the sim-
260   ulated surface temperature has a smaller positive bias of 0.73 K. Thus, MAR consistently simulates a stable regime with an average positive temperature gradient of 2.82 K. In fact, the observations show a very small temperature gradient (well-mixed neutral stratification) during winter at EGRIP. Contrary to summer, when both MAR and the observations show a slightly stable regime and their flux magnitudes are similar, MAR overestimates the magnitude of the (mostly depositional) flux in winter due to the strong stratification. A plausible explanation for the observed neutral atmospheric conditions during winter could be the
265   dominating effect of mixing by katabatic winds at EGRIP, which might not be accurately captured by MAR.

    We find that the systematic error of the LHF simulation in MAR is a consequence of a systematic error in Δq. The humidity gradient is not only impacted by the temperature gradient itself but also by the absolute temperature values. Because of the non-linear relationship between temperature and specific humidity (Clausius-Clapeyron relationship), even if the temperature
270   gradient and the relative humidity were perfectly captured, a bias in both surface and 2 m air temperature would cause a bias in Δq. Additionally, a bias in the temperature gradient causes a deviating magnitude of the humidity flux. We, therefore, argue that the bias correction b has to depend directly on the saturation specific humidity to characterize the non-linear dependence of the specific humidity on the temperature. Similarly, the factor correction m has to depend on the inverse of the saturation specific humidity because an overestimation of the humidity gradient needs counteracting by smaller values of m.

275

    Two choices to set up the simulations were made that have a direct impact on the LHF simulation. First, we found the default roughness length parameterization in MAR unsuitable for the smooth surface in the accumulation zone of the GrIS, producing consistently too high roughness length values and, consequently, reduced wind speeds. For lack of a better parameterization, we use a fixed roughness length of $1.3 \cdot 10^{-4}$ m throughout the entire simulation period. This value corresponds to the median
280   of direct EC at EGRIP in the summer of 2019 (Steen-Larsen and Wahl, 2021) and agrees with EC measurements from the katabatic wind zone of the Antarctic Ice Sheet ($z_0 = 1.6 \cdot 10^{-4}$ m, Van den Broeke et al., 2005). There are no measurements of the roughness length at EGRIP available in winter. However, we are confident that the chosen roughness length is suitable for simulations in the accumulation zone of the GrIS year-round as the resulting wind speeds are consistent with the observations (Fig. A7). Second, we turned off blowing snow in the simulations to avoid local SMB variations and to exclude redistribution
285   of deposited snow from the SMB input. Disregarding blowing snow in the simulations supports the validity of our results for

larger parts of the ice sheet. However, Le Toumelin et al. (2021) find that blowing snow and associated blowing snow sublimation improves MAR's ability to capture the surface energy and mass balance more accurately. Their simulations indicate that blowing snow decreases the LHF. It should therefore be taken into account when estimating the contribution of the humidity flux to the SMB in regions that are prone to blowing snow and with relatively little accumulation, such as the Antarctic
290 accumulation zone. We consider the effect of blowing snow on the humidity flux simulation to have limited impact on our results, as at EGRIP, the annual accumulation is comparably high and assuming that blowing snow events are rare. Including the effects of blowing snow, as well as better representing the LHF and its contribution to the SMB, requires datasets from an observational network covering the accumulation zone of the GrIS.

295 Our study documents large uncertainties in the SMB contribution of the humidity flux, as even the net humidity flux direction (mass loss or gain) switches after correcting the humidity fluxes. On multi-annual time scales, even small systematic errors in the humidity flux simulation have large impacts on the simulation of the net SMB. In MAR, the LHF has a correlation radius ($R \geq 0.5$) of 450 km, indicating that the results of this study are also valid for wider areas of the accumulation zone. In the present climate, our simulations suggest that the sublimation and deposition cancel each other out to a large degree.
300 As a consequence, the net current sublimation contribution to the total annual SMB is small. However, the balance between sublimation and deposition might shift in a warming climate. Simulations by Cullen et al. (2014) for the accumulation zone of the GrIS suggest that the domination of sublimation over deposition will increase in a warmer climate. As a consequence, the net contribution of the humidity flux to the SMB would increase and could gain importance in the accelerating mass loss of the GrIS. We show that systematic errors in the humidity flux change MAR's simulation of the SMB in the long term. Thus,
305 detailed uncertainty studies concerning the humidity flux need to accompany simulations over long time periods, such as to estimate the accumulation zone extent or in ice sheet stability climate predictions.

4 Conclusions

This study aims to provide a reliable estimate of the humidity flux contribution to the SMB in the accumulation zone of the GrIS. This is achieved by combining simulations of the regional climate model MAR with a new dataset of high-resolution
310 EC flux measurements. We evaluated the LHF in the MAR model simulation with four years of continuous meteorological observations at the EGRIP location. In summer, MAR reproduces the magnitude, distribution, and diurnal cycle remarkably well but has a bias in the LHF towards a negative (depositional) flux of -1.3 W m^{-2}. In winter, MAR consistently overestimates the magnitude of the LHF. Both the summer bias and the winter overestimation for the LHF are caused by systematic errors in Δq. The humidity gradient depends non-linearly on the surface and 2 m air temperature, as well as the resulting gradient. We,
315 therefore, proposed a simple linear correction function for the simulated LHF based on the surface saturation specific humidity in MAR to account for this non-linear temperature-humidity relationship. After correcting the systematic errors in the model data, the net humidity flux is estimated to account for about -1 % of the total SMB compared to +5.6 % for the uncorrected simulation. However, the contribution of the humidity flux to the SMB shows large seasonal variations. During summer, the

net humidity flux accounts for 32 % of the total SMB, 31 % of the total mass gain is sublimated again, and vapor deposition accounts for 9.6 % of the total mass gain. Our results thus demonstrate that the humidity flux plays a major role in the composition of the summer SMB.

Despite the relatively small value of the contribution from the humidity flux to the SMB on intra-annual time-scales, snow parameters used as climate proxies, such as snow structure, impurities, and water stable isotopes, can be influenced by sublimation and deposition even on such short time-scales. Recent research has documented (Hughes et al. (2021), Wahl et al. (2022)) that sublimation has the potential to overwrite the initial precipitated climate signal in the isotopic composition. Being able to simulate the humidity flux accurately throughout the year is critical for interpreting the proxy climate signal. This study provides a robust and simple way to correct systematic, temperature-driven errors in the humidity flux simulation in the polar regional climate model MAR. The achieved accuracy of the corrected humidity flux opens the opportunity to use MAR for future investigations of how the atmosphere-snow humidity exchange influences the surface snow.

Data availability. The PROMICE AWS product is available at https://doi.org/10.22008/promice/data/aws (Fausto et al., 2019). The EC water vapor flux data set is available in PANGEA (Steen-Larsen et al., 2022). The MAR simulations that are part of this publication are currently in the process of being uploaded to Pangaea and will be publicly available upon publishing.

Appendix A
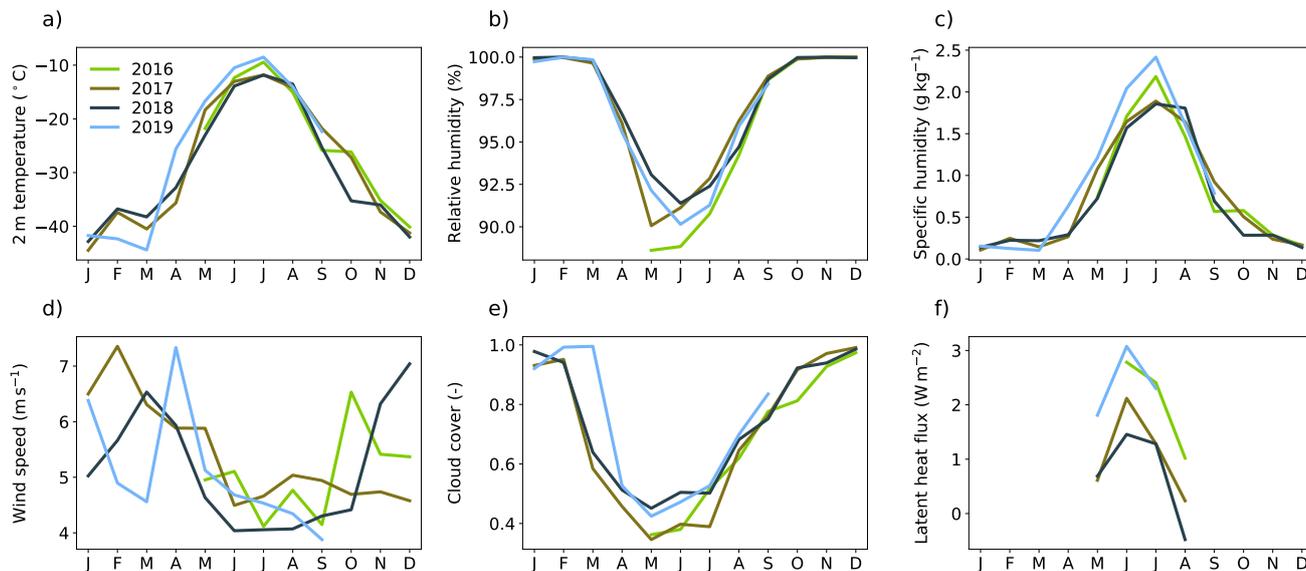
Figure A1. Monthly mean seasonal cycles of different meteorological variables (a-e) for the individual years in the observational period (2016-2019). All meteorological data is obtained from the AWS except for the latent heat flux that is observed with an EC system (f).
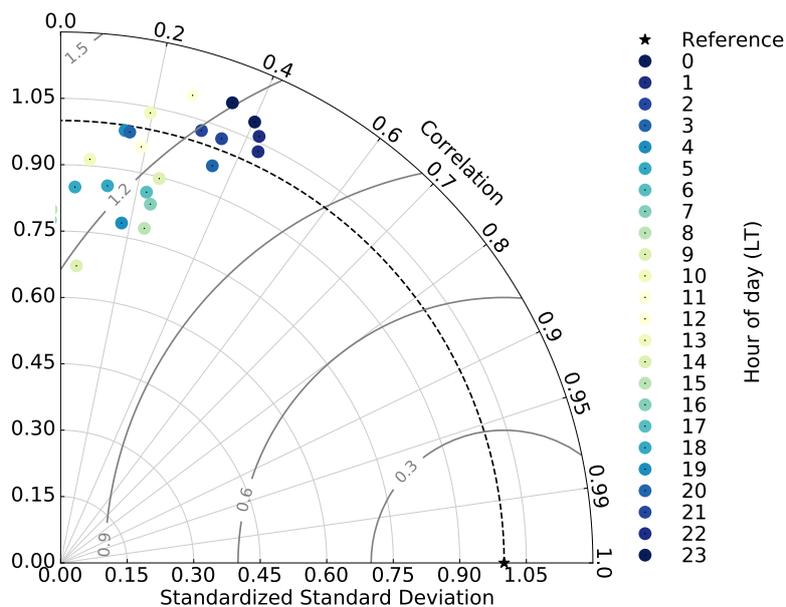
Figure A2. Taylor diagram of the summer latent heat flux averaged for every individual hour of the day. The reference is the EC LHF measurements for all four summers. Dark colors correspond to night hours and bright colors to day hours. The gray circles correspond to the relative error. LT is UTC-2.
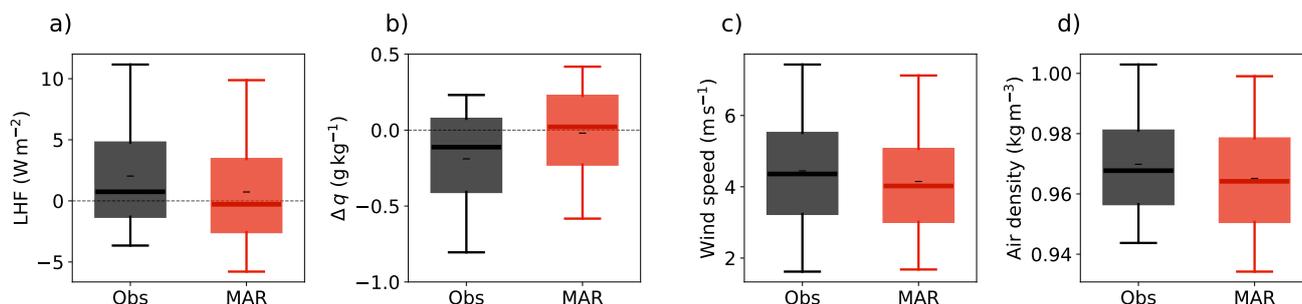
Figure A3. Distribution of the latent heat flux (a), specific humidity gradient (Δq, b), wind speed (c), and air density (d) for all summers (June, July) in 2016–2019 from observations (Obs, black) and (MAR, red). Black dashes (-) denote the mean, thick lines denote the median, boxes denote the 25th–75th percentile, and whiskers denote the 5th–95th percentile.
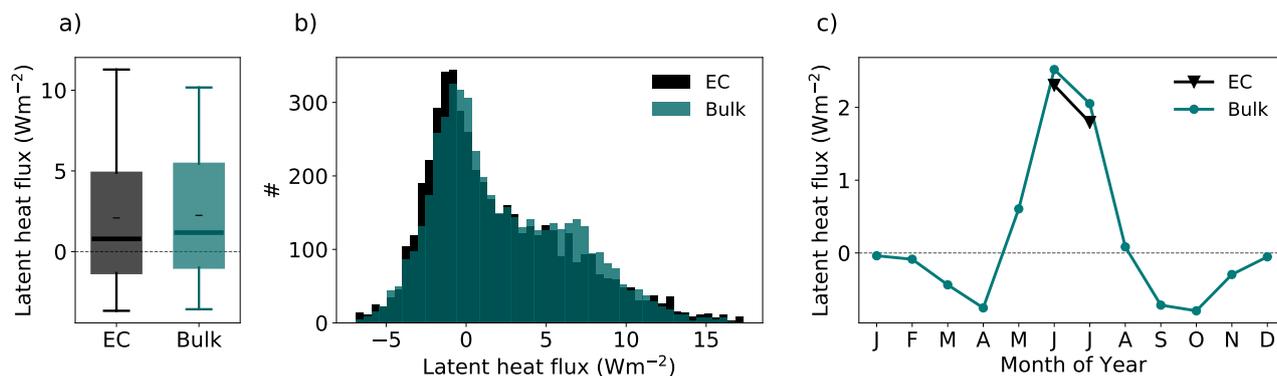
Figure A4. Comparison of the direct EC LHF measurements (black) to the bulk calculation of the LHF from meteorological observations (turquoise) using a constant roughness length of $1 \cdot 10^{-5}$ m in distribution (left, middle), and monthly mean seasonal cycle (right) for all summer months (June, July) in 2016–2019. In (a), black dashes (-) denote the mean, thick lines denote the median, boxes denote the 25th–75th percentile, and whiskers denote the 5th–95th percentile.
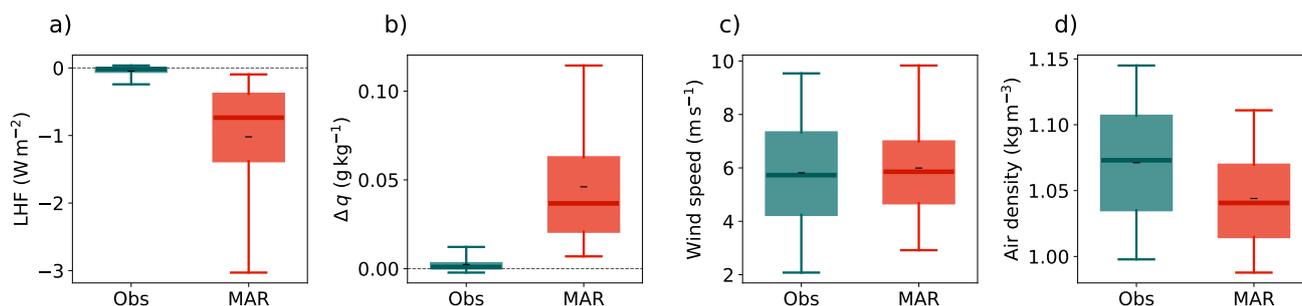
Figure A5. Like Fig. A3, but for all winters (December, January).
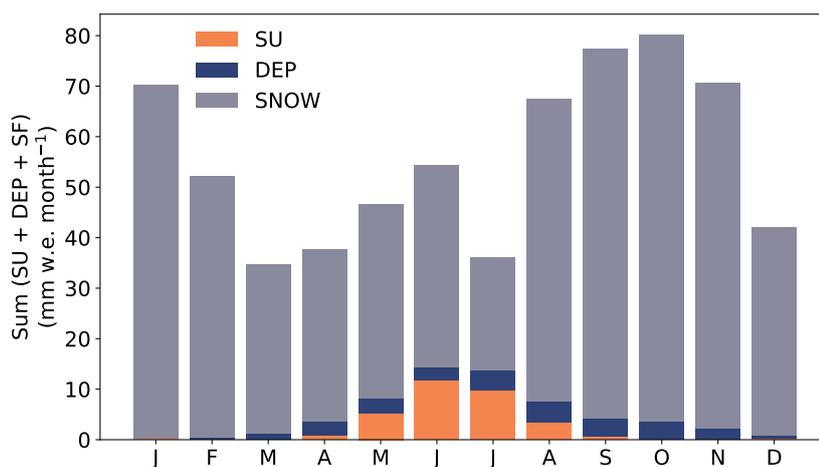
Figure A6. Components of the SMB, sublimation (SU, orange), deposition (DEP, blue), and snowfall (SNOW, grey), at the EGRIP site simulated with MAR for all months of the year in 2016–2019. The correction function (Sec. 3.2) is applied to the humidity flux.
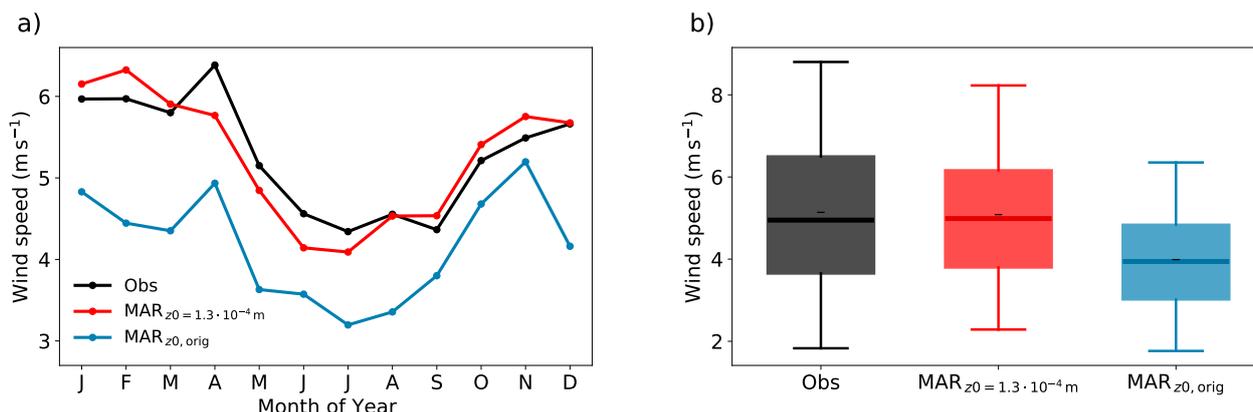
Figure A7. Sesonal cycle (a) and distribution (b) of the wind speed from observations (black, Obs), and in MAR using a fixed roughness length of $z_0 = 1.3 \cdot 10^{-4}$ m (red, MAR$_{z0=1.3\cdot10^{-4}\,\text{m}}$) and using the implemented roughness length parameterisation (blue, MAR$_{z0,\text{orig}}$). In (b), black dashes (-) denote the mean, thick lines denote the median, boxes denote the 25th–75th percentile, and whiskers denote the 5th–95th percentile.
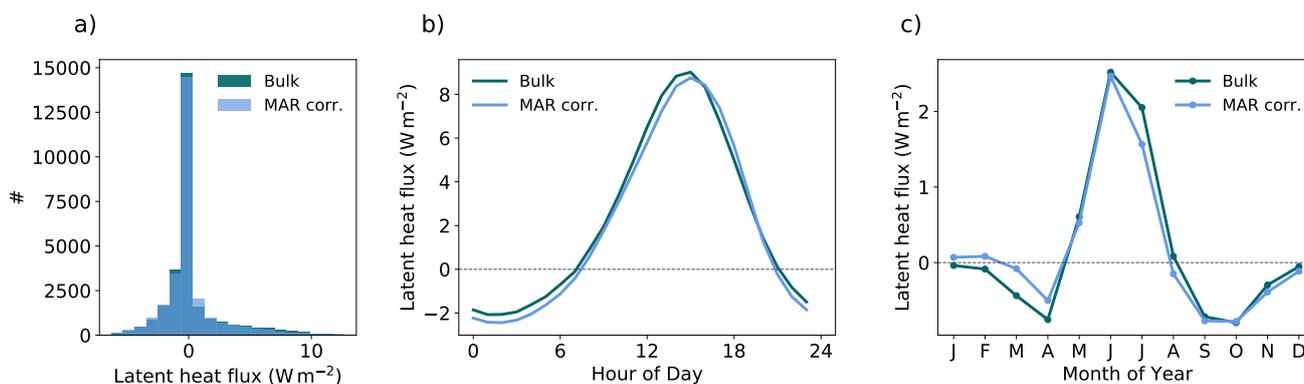
Figure A8. (a) Hourly data distribution in the observational period (05/2016–08/2019), (b) diurnal cycle in summer (June, July) and (c) monthly mean seasonal cycle of the bulk estimated latent heat flux from meteorological observations (turquoise, Bulk) and the corrected simulated latent heat flux in MAR (blue, MAR corr.).

Author contributions. HCSL and LJD conceived the study. XF and LJD ran the MAR model simulations. SW and HC obtained the EC observational dataset. LJD did the formal analysis with contributions from HCSL and SW. Investigations were done by LJD with contributions from all co-authors. LJD wrote the manuscript with contributions of AKF and HCSL. Reviews and edits are made by all co-authors. Visualisation is made by LJD. The study was supervised by HSCL and AKF. HCSL acquired funding for this study and administrated the project.

Competing interests. At least one of the (co-)authors is a member of the editorial board of *The Cryosphere*.

Acknowledgements. This paper has received funding from the European Research Council (ERC) under the European Union's Horizon 2020 research and innovation program: Starting Grant SNOWISO (grant agreement no. 759526). AWS data from the Programme for Monitoring of the Greenland Ice Sheet (PROMICE) and the Greenland Analogue Project (GAP) were provided by the Geological Survey of Denmark and Greenland (GEUS) at https://www.promice.org. EGRIP is directed and organized by the Centre for Ice and Climate at the Niels Bohr Institute, University of Copenhagen. It is supported by funding agencies and institutions in Denmark (A. P. Møller Foundation, University of Copenhagen), USA (US National Science Foundation, Office of Polar Programs), Germany (Alfred Wegener Institute, Helmholtz Centre for Polar and Marine Research), Japan (National Institute of Polar Research and Arctic Challenge for Sustainability), Norway (University of Bergen and Trond Mohn Foundation), Switzerland (Swiss National Science Foundation), France (French Polar Institute Paul-Emile Victor, Institute for Geosciences and Environmental research), Canada (University of Manitoba) and China (Chinese Academy of Sciences and Beijing Normal University). We thank Mike Town for valuable input.

References

Amory, C., Kittel, C., Le Toumelin, L., Agosta, C., Delhasse, A., Favier, V., and Fettweis, X.: Performance of MAR (v3. 11) in simulating the drifting-snow climate and surface mass balance of Adélie Land, East Antarctica, Geoscientific Model Development, 14, 3487–3510, 2021.

Andreas, E. L.: A theory for the scalar roughness and the scalar transfer coefficients over snow and sea ice, Boundary-Layer Meteorology, 38, 159–184, 1987.

Baldocchi, D.: A multi-layer model for estimating sulfur dioxide deposition to a deciduous oak forest canopy, Atmospheric Environment (1967), 22, 869–884, 1988.

Boisvert, L. N., Lee, J. N., Lenaerts, J. T., Noël, B., van den Broeke, M. R., and Nolin, A. W.: Using remotely sensed data from AIRS to estimate the vapor flux on the Greenland ice sheet: Comparisons with observations and a regional climate model, Journal of Geophysical Research: Atmospheres, 122, 202–229, 2017.

Box, J. E. and Steffen, K.: Sublimation on the Greenland ice sheet from automated weather station observations, Journal of Geophysical Research: Atmospheres, 106, 33 965–33 981, 2001.

Casado, M., Landais, A., Picard, G., Arnaud, L., Dreossi, G., Stenni, B., and Prié, F.: Water isotopic signature of surface snow metamorphism in Antarctica, Geophysical Research Letters, 48, e2021GL093 382, 2021.

Cullen, N. J. and Steffen, K.: Unstable near-surface boundary conditions in summer on top of the Greenland Ice Sheet, Geophysical Research Letters, 28, 4491–4493, 2001.

Cullen, N. J., Steffen, K., and Blanken, P. D.: Nonstationarity of turbulent heat fluxes at Summit, Greenland, Boundary-layer meteorology, 122, 439–455, 2007.

Cullen, N. J., Mölg, T., Conway, J., and Steffen, K.: Assessing the role of sublimation in the dry snow zone of the Greenland ice sheet in a warming world, Journal of Geophysical Research: Atmospheres, 119, 6563–6577, 2014.

Fausto, R., van As, D., and Mankoff, K.: Programme for monitoring of the Greenland ice sheet (PROMICE): Automatic weather station data, Version: v03 [data set], Geological survey of Denmark and Greenland (GEUS), https://doi.org/10.22008/promice/data/aws, 2019.

Fausto, R. S., van As, D., Mankoff, K. D., Vandecrux, B., Citterio, M., Ahlstrøm, A. P., Andersen, S. B., Colgan, W., Karlsson, N. B., Kjeldsen, K. K., et al.: Programme for Monitoring of the Greenland Ice Sheet (PROMICE) automatic weather station data, Earth System Science Data, 13, 3819–3845, 2021.

Fettweis, X.: Reconstruction of the 1979–2006 Greenland ice sheet surface mass balance using the regional climate model MAR, The Cryosphere, 1, 21–40, 2007.

Fettweis, X., Gallée, H., Lefebre, F., and van Ypersele, J.-P.: Greenland surface mass balance simulated by a regional climate model and comparison with satellite-derived data in 1990–1991, Climate Dynamics, 24, 623–640, 2005.

Fettweis, X., Box, J. E., Agosta, C., Amory, C., Kittel, C., Lang, C., van As, D., Machguth, H., and Gallée, H.: Reconstructions of the 1900–2015 Greenland ice sheet surface mass balance using the regional climate MAR model, The Cryosphere, 11, 1015–1033, 2017.

Fettweis, X., Hofer, S., Krebs-Kanzow, U., Amory, C., Aoki, T., Berends, C. J., Born, A., Box, J. E., Delhasse, A., Fujita, K., et al.: GrSMB-MIP: intercomparison of the modelled 1980–2012 surface mass balance over the Greenland Ice Sheet, The Cryosphere, 14, 3935–3958, 2020.

Fox-Kemper, B., Hewitt, H., Xiao, C., Aðalgeirsdóttir, G., Drijfhout, S., Edwards, T., Golledge, N., Hemer, M., Kopp, R., Krinner, G., Mix, A., Notz, D., Nowiciki, S., Nurhati, I., Ruiz, J., Sallée, J., Slangen, A., and Yu, Y.: Chapter 9: Ocean, Cryosphere and Sea Level Change, vol. 2018, https://doi.org/10.1017/9781009157896.011.1212, 2021.

390 Gallée, H., Guyomarc'h, G., and Brun, E.: Impact of snow drift on the Antarctic ice sheet surface mass balance: possible sensitivity to snow-surface properties, Boundary-Layer Meteorology, 99, 1–19, 2001.

Goelzer, H., Nowicki, S., Payne, A., Larour, E., Seroussi, H., Lipscomb, W. H., Gregory, J., Abe-Ouchi, A., Shepherd, A., Simon, E., et al.: The future sea-level contribution of the Greenland ice sheet: a multi-model ensemble study of ISMIP6, The Cryosphere, 14, 3071–3096, 2020.

395 Hersbach, H., Bell, B., Berrisford, P., Hirahara, S., Horányi, A., Muñoz-Sabater, J., Nicolas, J., Peubey, C., Radu, R., Schepers, D., et al.: The ERA5 global reanalysis, Quarterly Journal of the Royal Meteorological Society, 146, 1999–2049, 2020.

Holtslag, A. and De Bruin, H.: Applied modeling of the nighttime surface energy balance over land, Journal of Applied Meteorology and Climatology, 27, 689–704, 1988.

Hughes, A. G., Wahl, S., Jones, T. R., Zuhr, A., Hörhold, M., White, J. W., and Steen-Larsen, H. C.: The role of sublimation as a driver of
400 climate signals in the water isotope content of surface snow: Laboratory and field experimental results, The Cryosphere, 15, 4949–4974, 2021.

Le Toumelin, L., Amory, C., Favier, V., Kittel, C., Hofer, S., Fettweis, X., Gallée, H., and Kayetha, V.: Sensitivity of the surface energy budget to drifting snow as simulated by MAR in coastal Adelie Land, Antarctica, The Cryosphere, 15, 3595–3614, 2021.

Mouginot, J., Rignot, E., Bjørk, A. A., Van den Broeke, M., Millan, R., Morlighem, M., Noël, B., Scheuchl, B., and Wood, M.: Forty-six
405 years of Greenland Ice Sheet mass balance from 1972 to 2018, Proceedings of the national academy of sciences, 116, 9239–9244, 2019.

Paulson, C. A.: The mathematical representation of wind speed and temperature profiles in the unstable atmospheric surface layer, Journal of Applied Meteorology and Climatology, 9, 857–861, 1970.

Schlögl, S., Lehning, M., Nishimura, K., Huwald, H., Cullen, N. J., and Mott, R.: How do stability corrections perform in the stable boundary layer over snow?, Boundary-Layer Meteorology, 165, 161–180, 2017.

410 Sigmund, A., Dujardin, J., Comola, F., Sharma, V., Huwald, H., Melo, D. B., Hirasawa, N., Nishimura, K., and Lehning, M.: Evidence of Strong Flux Underestimation by Bulk Parametrizations During Drifting and Blowing Snow, Boundary-Layer Meteorology, 182, 119–146, 2022.

Steen-Larsen, H. C. and Wahl, S.: 2m processed sensible and latent heat flux, friction velocity and stability at EastGRIP site on Greenland Ice Sheet, summer 2019, https://doi.org/10.1594/PANGAEA.928827, 2021.

415 Steen-Larsen, H. C., Wahl, S., Box, J. E., and Hubbard, A. L.: Processed sensible and latent heat flux, friction velocity and stability at EastGRIP site on Greenland Ice Sheet, https://doi.org/10.1594/PANGAEA.946741, 2022.

Steffen, K., Box, J., and Abdalati, W.: Greenland climate network: GC-Net, US Army Cold Regions Reattach and Engineering (CRREL), CRREL Special Report, pp. 98–103, 1996.

Town, M. S. and Walden, V. P.: Surface energy budget over the South Pole and turbulent heat fluxes as a function of an empirical bulk
420 Richardson number, Journal of Geophysical Research: Atmospheres, 114, 2009.

Van den Broeke, M., Van As, D., Reijmer, C., and Van de Wal, R.: Sensible heat exchange at the Antarctic snow surface: a study with automatic weather stations, International Journal of Climatology: A Journal of the Royal Meteorological Society, 25, 1081–1101, 2005.

Wahl, S., Steen-Larsen, H., Hughes, A., Dietrich, L., Zuhr, A., Behrens, M., Faber, A.-K., and Hörhold, M.: Atmosphere-Snow Exchange Explains Surface Snow Isotope Variability, Geophysical Research Letters, p. e2022GL099529, 2022.

425   Zolles, T. and Born, A.: Sensitivity of the Greenland surface mass and energy balance to uncertainties in key model parameters, The Cryosphere, 15, 2917–2938, 2021.